Measurements of Transport due to Low Frequency Oscillations in a Rotating Hollow Cathode Plasma

IEPC-2015-137／ISTS-2015-b-137

Presented at Joint Conference of 30th International Symposium on Space Technology and Science, 34th International Electric Propulsion Conference and 6th Nano-satellite Symposium
Hyogo-Kobe, Japan
July 4–10, 2015

Taylor S. Matlock[*], Christopher A. Dodson[†], Dan M. Goebel[‡], and Richard E. Wirz[§]
University of California Los Angeles, Los Angeles, CA, 90095, USA

We investigate the contribution of a coherent, low-frequency $m = 1$ oscillation to cross-field electron transport in a hollow cathode discharge with a cylindrical anode through the measurement of correlated plasma density and potential oscillations. A cylindrical electrode is instrumented with wall probes to measure the azimuthal distribution of radial electron current to the boundary through time. Electrostatic probes are inserted into the plasma contained within the electrode to monitor correlated disturbances in the plasma potential, density, and ion rotation rate. Through a simple reconstruction of a representative spatio-temporal evolution we demonstrate that this mode may be the main source of cross-field electron transport in this device at the measured conditions.

I. Introduction

Hollow cathodes have long played a crucial role in plasma propulsion devices, providing the electron current necessary to sustain a discharge in both ion engines and Hall effect thrusters. There have been numerous studies on instabilities associated with hollow cathode operation in various discharge configurations.[1–7] One such configuration utilizes a cylindrical anode, coaxial with the cathode and a solenoid-driven magnetic field, allowing for relatively high ionization fractions through radial confinement of electrons. This configuration, with a radial electric field and density gradient across an axial magnetic field, leads to rotating instabilities.[8,9]

The device studied here comprises the plasma delivery system of the Plasma interactions (Pi) facility at UCLA, designed for the testing of advanced materials for applications in harsh environments, similar to that produced in electric propulsion and pulsed power systems.[10] Plasma is generated by a hollow cathode discharge with a cylindrical anode, axial magnetic field and electron reflexing from a target 1 m downstream of the cathode exit.

Previous studies on this device show the onset of coherent oscillations in the plasma potential near the anode when the cylindrical anode is insulated from the plasma by an axial magnetic field.[11] The radial electric field within 1 cm of the anode walls changes from pointing outward to inward as the magnetic field is brought on, and the density profile flattens radially as the magnetic field is increased. High amplitude potential oscillations are measured off-axis, with a frequency in the 10-20 kHz range that is an increasing function of magnetic field strength. Further studies revealed these to be $m = 1$ oscillations in the $\mathbf{E} \times \mathbf{B}$ direction, that exhibit a nearly linear azimuthal mode dispersion at moderate magnetic field strengths and increase in frequency with increasing discharge current.[12]

[*]Postdoctoral Researcher, Dept. of Mechanical and Aerospace Engineering , tmatlock17@ucla.edu.
[†]Ph.D. Candidate, Dept. of Mechanical and Aerospace Engineering
[‡]Adjunct Professor, Dept. of Mechanical and Aerospace Engineering
[§]Associate Professor, Dept. of Mechanical and Aerospace Engineering

In the following we describe experiments using translating probes to measure the correlation between the azimuthal fluctuations in density and potential caused by the low frequency, $m = 1$ mode. The net radial electron flux due to the $E_\theta \times B_z$ drift is calculated and compared to time resolved measurements of the electron current collected by azimuthally spaced wall probes on a cylindrical electrode. We find that, with proper corrections of the probe signals, the calculated radial current due to the $m = 1$ mode can account for all but a moderate DC offset in the electron current to the wall probes.

II. Experimental Apparatus

The Pi facility[10] is comprised of a 1.8 m diameter by 2.8 m long vacuum chamber evacuated by dual cryopumps with a combined pumping speed of 5000 L/s on argon, allowing base pressures as low as 5 x 10^{-7} Torr. The plasma source (a 250 A LaB_6 hollow cathode coaxial with a 30 cm long cylindrical copper anode) is mounted on one flange of the chamber, diametrically opposed to the flange which supports the target. Intermediate guide magnets are mounted to struts lying chordally across the bottom of the chamber. All components of the plasma source and delivery system lie within the vacuum chamber with small axial gaps between system elements allowing for the insertion of plasma diagnostics in a flexible manner.

An axial magnetic field is supplied by solenoids wound on the cylindrical copper electrodes. A 1.5 cm wide section of copper tubing, placed in a 2 cm gap between two 30 cm long guide magnets, was equipped with copper wall probes, placed on the outer wall of the tube (insulated by a thin Kapton sheet) to view the plasma through 4.7 mm bores. A sketch of the setup is shown in Fig. 1a. The current to each wall probe, as well as to the probe ring itself is measured across 11 Ω shunt resistors on a National Instruments PXIe-4300 module. There are 8 bores in the probe ring; 7 are equipped with wall probes and one is left open for insertion of translating probes (this has been an emissive probe, cylindrical Langmuir probe and Mach probe on separate occasions, all of which are described below).

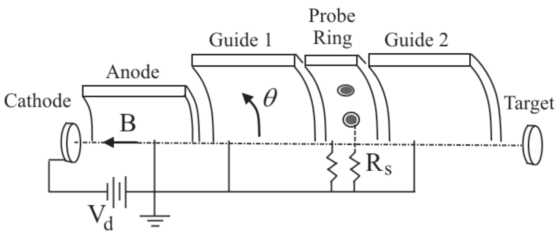

(a)

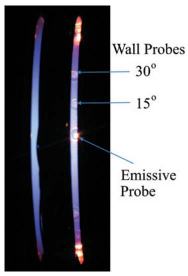

(b)

Figure 1: (a) Sketch of experimental setup (not to scale) (b) Probe ring and emissive probe during experiment

Here we present results from a single test condition. We have 7 sccm of xenon flow through a ring injector between cathode and anode and 5 sccm of xenon flowing axially through the hollow cathode itself resulting in a background pressure of $9{\times}10^{-5}$ Torr corrected for xenon. The discharge runs current-limited at 25 A (14 A is collected by the anode, 11 A by the two guide rings) with a steady discharge voltage of 30.7 V. A tungsten target sits roughly 1 m downstream of the cathode and floats to -37 V, reflecting any cathode-emitted electrons that can span the device. The magnetic field strength in the region of the probe ring is 250 G on axis.

A. Plasma Diagnostics

Translating probes include a floating emissive probe, a cylindrical Langmuir probe and a Mach probe. The first two are used to measure the cross-phase in density and potential oscillations (this is taken to indicate whether the oscillations lead to transport) while the third is used to measure the ion rotation rate in the azimuthal direction (to check for a correlation with the oscillation frequency as suggested by Sakawa *et al*[13]). All measurements reported here are taken at 200 kHz over a 1 second sample at each probe location, using an isolated NI PXIe-4300.

1. *Emissive Probe*

Plasma potential profiles (up to a near unity factor of electron temperature) are measured by a floating emissive probe on a 600 Ω resistor bridge across the DC heater power supply (an EA-3025S chosen for its low stray capacitance) terminals. The floating emissive probe consists of a 2 mm diameter tube of double bore alumina with a 0.13 mm diameter tungsten filament attached to tantalum leads and protruding in a roughly 5 mm diameter semicircle.

As the emissive probe is heated past a threshold temperature it begins to emit an electron current, causing it to float at a potential closer to that of the surrounding plasma. When the probe is emitting enough electrons the plasma sheath may become space charge saturated and no further electron current will be drawn from the filament to the plasma. At saturation the probe floats a factor near unity of the electron temperature below the plasma potential.[14,15] One can then monitor the floating potential of an emissive probe heated well into the space charge saturated limit in order to estimate the local plasma potential if the electron temperature (and the near unity factor) is known.

During the course of this study it became clear that the stray capacitance of the emissive probe circuit was high enough to act as a low pass filter to plasma potential oscillations when the resistance between probe tip and plasma was too large (e.g. when the emitted electron current was low).[16] The sheath resistance is very low when the emissive probe is heated to saturation and the stray capacitance becomes negligible. The low pass filtering of the cold (i.e. non-emitting) probe leads to a large difference in potential oscillation amplitude compared to the hot (i.e. emitting a saturated electron current) probe that can be mistaken for a high amplitude electron temperature oscillation.

$$\tilde{V}_f^h - \tilde{V}_f^c = i\omega C_f \frac{T_e}{eI_i}\tilde{V}_f^c + \frac{(\bar{V}_f^h - \bar{V}_f^c)}{T_e}\tilde{T}_e - \gamma\frac{T_e}{e}\frac{\tilde{n}_e}{n_e} \tag{1}$$

Researchers have used the difference in time-resolved potential measured by hot and cold probes to infer the time-resolved electron temperature.[17–19] We note in a recent paper[16] using a linear perturbation analysis ($\phi(t) = \bar{\phi} + \tilde{\phi}e^{-i\omega t}$) that the difference in potential oscillations measured by hot and cold probes may also be a strong function of density oscillations and circuit stray capacitance. This is shown in Eqn. (1), where $\tilde{V}_f^h$ and $\tilde{V}_f^c$ are the floating potential oscillations measured by the hot and cold emissive probes respectively, and it is assumed that the sheath resistance is negligible for the hot probe. Here, I_i is the ion current collected by the probe and γ is the ratio of emitted electron current to collected for the hot probe ($\gamma \sim 1$).

A precisely known or very low stray capacitance is necessary to determine the electron temperature fluctuations from the difference in hot and cold emissive probe signals using Eqn. 1. After calibrating for the stray capacitance in our measurement circuit (about 1 nF) we have estimated, through Eqn. 1, that the electron temperature fluctuations are of negligible amplitude, except very near the ring electrode wall, for the conditions described here.[16]

$$\tilde{V}_{pl} \approx \tilde{V}_f + \gamma\frac{T_e}{e}\frac{\tilde{n}_e}{n_e} \tag{2}$$

Plasma potential fluctuations are estimated from the saturated floating potential measurements of the hot probe using the same linear fluid theory, simplified in Eqn. 2 which neglects temperature fluctuations, and where we will assume $\gamma = 1$. Density fluctuations affect the floating potential oscillations of the hot probe in this analysis based on the assumed constancy of the electron current emitted by the probe. In order to collect net zero current (i.e. float) the potential of the filament must drop as the electron current from the plasma increases due to the density oscillation.

2. *Langmuir Probe*

Plasma density oscillations are characterized using a cylindrical Langmuir probe, with a 5.5 mm long section of 1.6 mm diameter tungsten rod exposed to the plasma, protruding from 3.1 mm diameter single bore alumina tube. The exposed section is 5 mm from the capped end of the alumina tube. This probe is biased 60 V below ground with a Kepco BOP-200 power supply to measure ion saturation current through a 10 Ω shunt resistor placed on the high side of the bias. Ion saturation current oscillations are considered to mainly reflect ion density fluctuations, though electron temperature and plasma potential oscillations may also affect the ion current. Emissive probe measurements suggest $\tilde{T}_e/T_e << \tilde{n}_i/n_i$ (as discussed above) and the Langmuir probe radius is much larger than the sheath, so we may confidently neglect these two effects.

3. Mach Probe

A Mach probe is utilized in these experiments to measure ion azimuthal rotation. The probe is constructed from 2 mm diameter, double bore alumina tubing with 2 mm long sections of exposed tungsten wire (0.25 mm diameter) facing opposite directions such that only a semicircular surface collects ions from either bore. Both electrodes are biased 60 V below anode potential to collect ion saturation current using the same Kepco BOP-200, with high side current measurements across 10 Ω shunt resistors.

There does not appear to be a consensus theory for cylindrical Mach probes in partially ionized plasmas with unmagnetized ions. In general Mach probe usage, the ratio of ion currents to upstream and downstream facing electrodes gives the ion Mach number ($M = v_i/c_s$) through the equation,

$$M = \frac{1}{K}\ln\left(\frac{I_{up}}{I_{down}}\right) \tag{3}$$

where K is some calibration factor that often depends on the ratio of ion to electron temperatures ($\tau \equiv T_i/T_e$). An extensive review of the various Mach probe theories is given by Chung, who shows a variety of fits for the calibration factor K.[20] Amongst these are PIC results from Hutchison for a sphere collecting unmagnetized ions that yield an average K of 1.34, which we adopt here. A kinetic model from Chung for a planar electrode suggests K may be as low as 1 when $\tau = 1$, which, if true, would mean our results using $K = 1.34$ may underestimate the ion Mach number by up to 25% (we do not expect to find $\tau > 1$ in our neutral-dominated plasma).

A further issue with prevailing Mach probe theory is the lack of time-dependence. Measurements shown here yield differing results for the ion rotation rate depending on how the time-averaging is performed. Taking the ratio of the time-averaged currents (i.e. $< I_{up} > / < I_{down} >$) yields a different, generally lower, estimate for the ion rotation than taking the time-average of the instantaneous current ratio (i.e. $< I_{up}/I_{down} >$). This results in a major source of uncertainty for the Mach probe results.

III. Experimental Results

An example of the electron current waveforms measured with the probe ring is shown in Fig. 2 along with the ion current wave measured by the cylindrical Langmuir probe placed at the inner radius of the ring through the bore at 0°. The azimuthal position of the wall probe nearest to the Langmuir probe is offset 15° in the $-\mathbf{E}\times\mathbf{B}$ direction ($\mathbf{B}$ points axially towards the cathode and $\mathbf{E}$ mostly points radially towards the axis). The waveforms in Fig. 2 show a pronounced $m = 1$ (e.g. for $\tilde{\phi} = \hat{\phi}e^{-i(\omega t - m\theta)}$), azimuthal current oscillation with a frequency of 12.2 kHz, traveling in the $+\mathbf{E}\times\mathbf{B}$ direction. This mode was also measured upstream, between the anode and the first guide cylinder in a previous study.[12] Figure 2 shows that this mode is superposed by both higher and lower frequency oscillations as it traverses the ring azimuthally. The high and low frequency modes are seen in the ring electrode current, while the $m = 1$ mode is not, suggesting the modulations are m=0 modes.

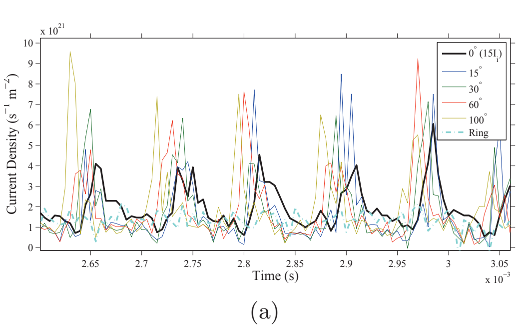

(a)

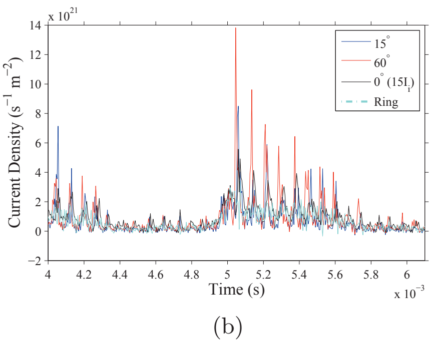

(b)

Figure 2: Current waveforms from Langmuir probe in ion saturation (0°), 4 azimuthally spaced wall probes and the ring electrode itself. The ion saturation current is multiplied by 15.

Power spectral densities for the various probe signals are collected in Fig. 3. The power spectra comparison in Fig. 3a is with the Langmuir and emissive probe signals at the position $x = R$ for direct correlation to the wall probe and ring electrode signals. The ring is dominated by DC and broad fluctuations ∼2 kHz, with a slight peak at the frequency of the azimuthal mode (due either to the wall probe bores or some misalignment with the magnetic field) and white noise at all other frequencies. A peak near 84 kHz is clear in the azimuthally distinct probes, and is prominent in the floating potential oscillations. Spatial power spectral density contours in Figs. 3b & 3c show that the higher frequency (84 kHz) mode has a peak power closer to the axis than the $m = 1$ mode at 12.2 kHz (and its associated harmonics). Harmonics of the 12.2 kHz mode appear to dominate at higher radii, suggesting the oscillations become steeper away from the axis.

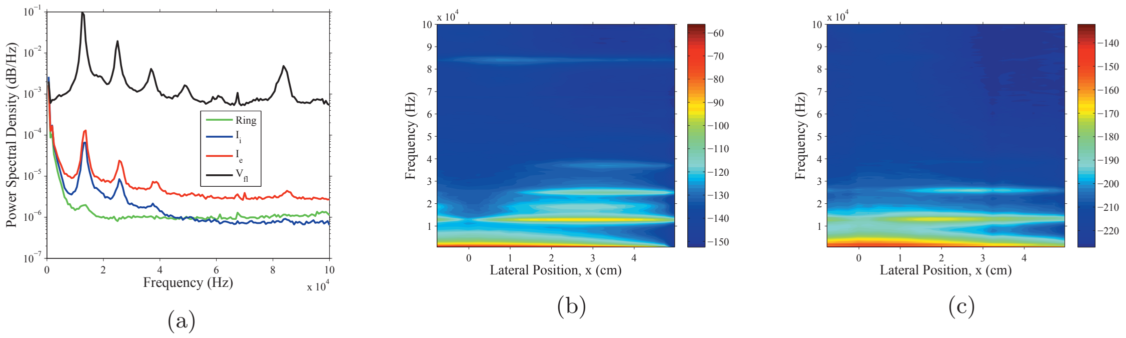

Figure 3: Power spectral densities (a) at $x = R$ comparing a wall probe with the ring electrode, Langmuir probe, and floating emissive probe, (b) for the floating emissive probe at various locations and (c) for the ion collecting Langmuir probe at various locations.

Time-averaged profiles measured by all three translating probes, showing ion density (assuming a constant $T_e = 4$ eV), plasma potential (within 1-2T_e), and azimuthal ion Mach number, are given in Fig. 4a. The Mach probe results reveal a constant rotation rate for ions near the axis, with an upturn in Mach number near the edge of the plasma that is suspected to correspond to a drop in the ion sound speed there rather than a shear in the rotation rate. The isorotation of ions agrees well with the theory of Davidson for Vlasov equilibria of unmagnetized ions in a parabolic potential well.[21]

Time-resolved measurements at each location of the translating probes are referenced to the wall probe 15° upstream in the $\mathbf{E} \times \mathbf{B}$ direction. The two-point dispersion relation between the translating probe and wall probe is found using the analysis method of Beall.[22] From the two-point dispersion we select the spectral power and phase for the 12.2 kHz, $m = 1$ mode for the profiles shown in Fig. 4b & 4c . The plasma potential oscillations are found by combining the saturated floating potential oscillation data with the ion density oscillation data from the Langmuir probe and the equation, $\tilde{V}_s = \tilde{V}_f + (T_e/e)\tilde{n}_i/n_i$, from the linear perturbation analysis.[16]

The fluctuation amplitudes in Fig. 4b are the square roots of the integrated spectral power density over the frequency band of interest based on Fourier decomposition. Plasma potential fluctuation power peaks near r=2.5-3 cm, while the density fluctuations (non-dimensionalized by the time-averaged density profile of Fig. 4a, reach a shallow peak near the ring electrode. Figure 4c shows the density oscillations lead the plasma potential by 100-150°, though this does not reflect the main trend observed in the waveforms. The plasma potential is actually quite constant over most of the 12 kHz cycle, with a sharp dip towards more negative potentials that precedes the sharp peaks in density observed on the Langmuir probe by over 30°. These trends are shown more clearly in the following section.

A. Transport Analysis

Correlated fluctuations in plasma potential and density may result in net electron transport across magnetic field lines. Here will we attempt to bound the degree to which the coherent, low frequency, $m = 1$ oscillations characterized in the preceding section are involved in driving electron currents across the magnetic field. Radial transport due to correlated azimuthal electric field and density perturbations can be estimated using,

$$< \tilde{n}\tilde{v}_{er} >= -\frac{1}{2B}\frac{m}{r}\left|\tilde{n}^*\tilde{\phi}\right|\cos\psi \tag{4}$$

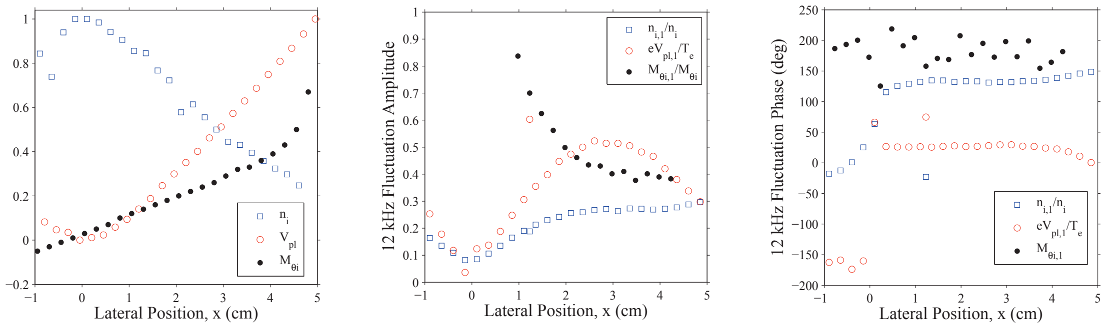

(a) (b) (c)

Figure 4: (a) Normalized, time-averaged profiles of ion density, plasma potential and azimuthal ion speed where the normalization values are 2.8×10^{17} m^{-3}, 8.5 V (where unity corresponds to -3.7 V) and 1 respectively. (b) Non-dimensionalized, RMS amplitude and (c) phase profiles for 12.2 kHz oscillations in ion density and plasma potential.

$$\psi = \arg(\tilde{n}^* \tilde{\phi} e^{i\pi/2}) \tag{5}$$

which may be found by taking the time average of second order terms in the quasi-linear perturbation analysis of the electron momentum equation. The tangential electric field at the conductor must go to zero, but this radial flux need only populate magnetic field lines near enough to the conductor that electrons can flow to it by other means.

Fourier analysis of our probe signals give $\left|\tilde{\phi}\right|$ =1.2 V, $|\tilde{n}| = 0.3n$ near the inner radius of the ring for the 12.2 kHz mode, with a phase difference of 150° (density peak leads potential peak), so that $\psi = 240°$. The time-averaged plots in Fig. 4a give $v_E = E_r/B_z$=7.2 km/s and $v_D = T_e \nabla n/nB_z$=3.2 km/s, while Eqn. (4) gives v_{er} ∼+70 m/s for an effective Hall parameter ($\Omega_{eff} \equiv v_{e\theta}/v_{er}$) of 150. The neutral density near the ring electrode may be as high as 6×10^{18} m^{-3} at these flow rates leading to a Hall parameter, $\Omega \equiv \omega_{ce}/\nu_{en}$, of as low as 3000, suggesting the azimuthal mode drives cross-field electron transport at least 20 times the classical levels.

An effective radial drift of 70 m/s, as estimated above, is insufficient to explain the high electron currents necessary to sustain the discharge. However, the radial drift speed need not be too large if the electron density is high enough on a magnetic field line that can connect electrons to the ring (e.g. through slight misalignment of the ring in the magnetic field). High densities at large radii may be enabled by the radial transport afforded by this azimuthal mode. At the peak fluctuation power (near $x = R/2 = 2.5$ cm) we find $\left|\tilde{\phi}\right|$ =2 V, $|\tilde{n}| = 0.3n$ and $\psi = 190°$, for an effective v_{er} of 430 m/s, which for the measured ion density of $3{\times}10^{17}$ m^{-3} leads to a radial current density, $2\pi r < \tilde{n}\tilde{v}_{er} >$ of 4 A/m. This is still nearly an order of magnitude too low sustain a 25 A discharge (total anode length is 0.9 m), though the ring electrode collects a time-averaged current of 8 A/m.

The linear analysis above assumes the azimuthal perturbations in plasma potential are of a single sinusoidal mode, while they may in fact be more resemblant of a sawtooth if the perturbation is a rotating double layer as seen in some magnetrons.[23] To determine a more accurate magnitude for the azimuthal electric field we start by reconstructing the time evolution of the radial plasma potential profile, using the technique described by Lobbia & Gallimore.[24] This consists of building transfer functions in Fourier space for each time series of the translating probe based on an input function, which in this case is the 15° wall probe electron current taken at the same time. The transfer function then allows us to build up a spatiotemporal map of the measured parameter, as in Fig. 5b, by applying the transfer function found at each location to a single input function. This is compared to a simpler technique, where we piece together small clips from each time series that are found to have the highest cross-correlation in wall probe current, shown in Fig. 5a.

Since the dominant oscillation is an $m = 1$ azimuthal mode, we can construct an instantaneous snapshot of the measured plasma parameter in the (r, θ) plane by assuming phase in the time series reconstruction

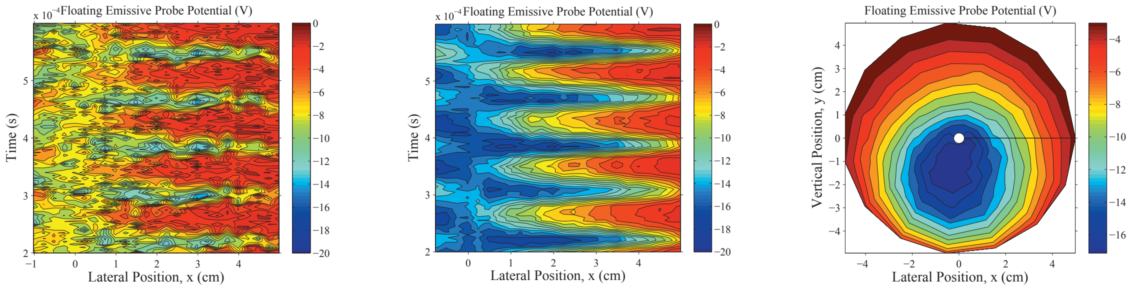

(a) (b) (c)

Figure 5: Reconstructed spatiotemporal evolution of floating emissive probe potential using (a) clips with the highest cross-correlation in wall probe current and (b) Fourier space transfer functions. (c) Instantaneous saturated floating potential in the probe plane assuming the time dependence in (b) is entirely due to $m = 1$ rotation.

in Fig. 5b is equivalent to θ, yielding the image in Fig. 5c. The reconstruction in Fig. 5c averages over 20 cycles of the spatiotemporal map in Fig. 5b, which is expected to help cancel out contributions from modes other than the $m = 1$ wave. Figure 5c shows clearly that the rotating (clockwise, in the $\mathbf{E} \times \mathbf{B}$ direction) potential well is deep enough to locally cut off the azimuthal E_r/B_z electron drift.

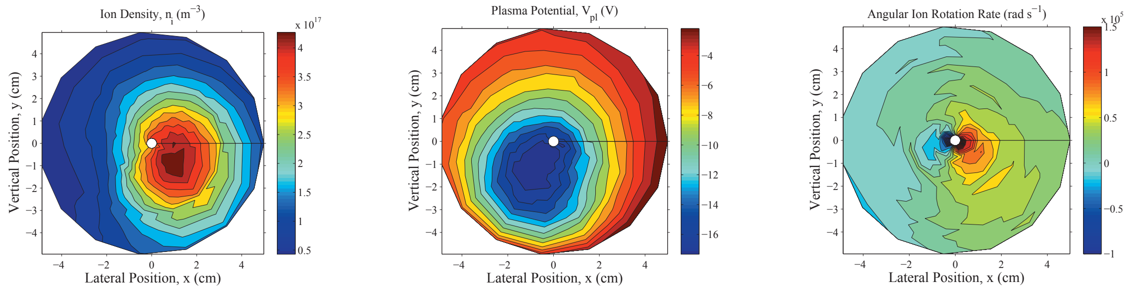

(a) (b) (c)

Figure 6: Instantaneous contours in the probe plane assuming all perturbations are $m = 1$ for (a) ion density (b) plasma potential and (c) angular ion rotation rate.

The (r, θ) reconstruction is used to qualitatively show the instantaneous structure of the plasma potential and density oscillations that constitute the 12.2 kHz, $m = 1$ mode in Fig. 6. Ion density contours in Fig. 6a are shown which assume a constant (spatial and temporal) electron temperature of 4 eV (based on Langmuir probe traces). The plasma potential map in Fig. 6b corrects the floating emissive probe potential with the $(T_e/e)\tilde{n}/n$ factor (using the ion density map of Fig. 6a) arising from the inability of the emissive probe to emit a large alternating electron current to match the oscillating electron flux impinging upon it.[16,25] Comparison of Fig. 6b with Fig. 5c shows how this correction factor amplifies the azimuthal electric field at 6 o'clock.

We note that this correction factor is derived assuming small amplitude perturbations, which is not the case for the measured potential oscillations which approach 10 V peak-to-peak inside a steady radial potential well of 8.5 V. However, as long as the density perturbations remain small (as in Fig. 4b) the correction factor should be the same for arbitrarily large voltage oscillations in the limit of negligible electron temperature fluctuations. This is again because the floating potential must adjust to the plasma potential such that the electron current collected by the probe remains constant in time (assuming the emitted current is relatively constant) even as the density fluctuates. To do so, it floats below the plasma potential by a factor $(T_e/e)\ln(1 + \tilde{n}/n)$ to within some constant for arbitrary plasma potential waveforms. The density fluctuations shown here remain below $\tilde{n}/n \approx 0.3$ so that $\ln(1 + \tilde{n}/n) = \tilde{n}/n$ within 15%.

Figure 6b indicates a strong E_θ pointing in the direction of the steady azimuthal electron drift near 6 o'clock and the necessary opposing E_θ near 9 o'clock. These azimuthal fields appear to affect the ion rotation shown in Fig. 6c, which indicates a peak rotation rate where the field points in the steady electron drift location, and a reversal in the rotation direction at 9 o'clock, where the electric field changes sign. The Mach probe theory utilized to predict Mach number from the ratio of upstream and downstream facing electrode currents comes from a steady-state model, so it is not clear whether the application of such a model is appropriate for the time-resolved analysis used to create Fig. 6c.

That the peak ion density occurs just upstream of the electric field at 6 o'clock (Fig. 6a) has important implications for the ability of this mode to drive net radial electron transport. The radial $E_\theta \times B_z$ drift points outwards at 6 o'clock and inwards at 9 o'clock, but the confluence of plasma near 6 o'clock suggests a net outward flow of electrons ought to occur. This effect can be seen in Fig. 7 where the results of Figs. 6a & 6b are used to estimate E_θ and $n_e E_\theta / B$.

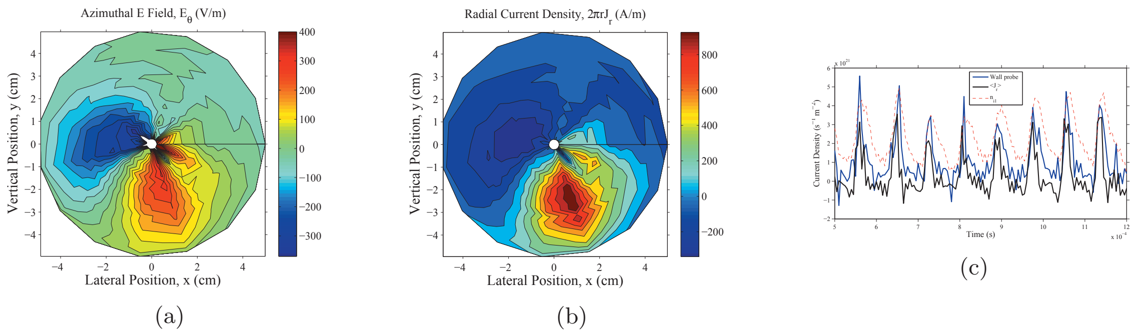

Figure 7: Instantaneous contours in the probe plane assuming all perturbations are $m = 1$ for (a) azimuthal E field (b) $2\pi r < nE_\theta > /B$. (c) Comparison of measured wall probe current waveform with predicted based on E_θ/B drift in (b) and with ion density fluctuations measured at $x = R$ multiplied by a constant (1.4x10^4) to share the same scale.

The azimuthal electric field estimates in Fig. 7a suggest positive field strengths in the 200-300 V/m range, compared to the linear estimates of <100 V/m used in the application Eqn. (4) above. The resultant radial electron current of Fig. 7b is substantial; possibly enough to maintain our 25 A discharge. To demonstrate this, the radial current to the wall probe location is estimated using $E_\theta^{j+1/2} = (V_{pl}^{j+1} - V_{pl}^{j})/(R\Delta\theta)$, where $\Delta\theta$ is the phase of the 12.2 kHz cycle at $t^{j+1/2}$, and $J_r^{j+1/2} = (E_{theta}^{j+1/2}/B)(n_i^{j+1} + n_i^{j})/2$. The result, in Fig. 7c, captures the measured peaks in wall probe current exceptionally well in most instances.

The ion saturation current to the Langmuir probe at $x = R$ is shown for comparison in Fig. 7c, to demonstrate that the prominent spikes in electron current during each cycle are more likely due to the radial $E \times B$ drift than due to some misalignment in the ring electrode causing field-aligned electron currents to reach the probe with peaks due to the rotating density perturbation.

In comparison to the current due to the $m = 1$ mode, the wall probe electron current has a DC offset near 7×10^{20} m^{-2} s^{-1}. Transport due to a single coherent oscillation cannot capture such an offset, because the azimuthal electric field must integrate to zero around a circumference. The DC offset may be related to the slight divergence of the magnetic field in the location of the ring electrode between solenoids. The magnetic field may be grazing the electrode at an angle of of nearly 6° according to magnetic field simulations, which would lead to a projected thermal electron flux (neglecting any electron repelling sheath) along the field of about 30×10^{20} m^{-2} s^{-1} based on the time-averaged electron density measured near the ring. More care may be needed in the experimental setup to discern the nature of the measured DC offset.

B. Instability

We have shown some of the characteristics of the $m = 1$ mode, but it remains to be demonstrated what drives and ultimately saturates this large amplitude instability in the conditions found in our device. The plasma parameters here are similar to those of Sakawa *et al*, where a similar fluctuation is labeled the Modified Simon-Hoh instability.[13] This instability is said to have a frequency equal to the ion rotation rate, which motivated the Mach probe measurements shown here.

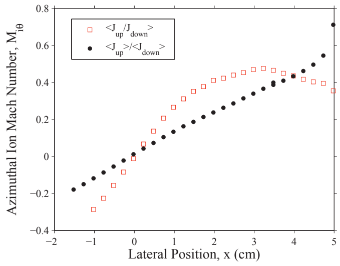

Figure 8: Ion azimuthal Mach number ($v_{i\theta}/c_s$) profiles for two different time-averaging schemes.

Mach probe results using the ratio of the time-averaged currents to the two electrodes suggest the ion rotation rate is only 2.7 kHz, far slower than the instability, but about equal to the ion gyrofrequency. However, the ion rotation rate obtained using the time-average of the instantaneous ratio of the two currents is much closer, around 8.3 kHz for radii inside of the potential oscillation amplitude peak. If a value of $K = 1$ instead of $K = 1.34$ is used in Eqn. 3, as discussed above, then the ion rotation rate is 11 kHz for T_e=4 eV (as assumed throughout this work) and 12.2 kHz (the frequency of the measured fluctuation) if T_e=5 eV.

It is unclear whether Mach probe theory should be expected to apply to the time-resolved data. The correspondence of a change in ion rotation direction with the change in azimuthal electric field sign in Figs. 6c & 7a is bolstering. However, the shear in the mean ion flow in Fig. 8 at higher radii is somewhat at odds with the constant frequency of the instability measured across this region if the dispersion relation of Sakawa applies.

The Modified Simon-Hoh instability is noted by Sakawa to fit into the broader class of anti-drift waves (where the frequency is inversely proportional to the diamagnetic drift frequency and thus largely proportional to B as observed in our experiments). The instability also fits well into the classification of Klose *et al* as an ion drift wave.[26] This instability is also marked by a phase speed equal to the ion azimuthal drift rate, exhibits a linear azimuthal dispersion and potential oscillations lag density by slightly less than 180°.

Regardless of the name of the instability, the basic mechanism is expected to be that familiar to a large class of cylindrical plasma instabilities: density perturbations lead to charge separation and thus azimuthal electric fields due to dissimilar azimuthal drifts for ions and electrons. If the electron drift is in the diamagnetic drift direction (and faster than the ions) the charge separation leads to an outward $E \times B$ drift and since the density is higher on the inboard side of the perturbation the loss of charged particles in this region is slower than the gain and the instability may be amplified. However, unless the axial wavelength of the instability is at least on the order of the device length, or the axial electron resistivity is high enough, electrons will be able to stream along field lines to shield out any region of excess ions and the instability will be damped.

IV. Conclusion

We have shown that a low frequency ($\omega_{ci} < \omega < \omega_{lh}$) $m = 1$ fluctuation can drive significant electron transport across an axial magnetic field in a cylindrical hollow cathode discharge. This is due to the co-location of an azimuthal electric field and a plasma density perturbation leading to a net outward $E_\theta \times B_z$ electron drift. The peak in radial transport due to the coherent oscillation occurs near the mid-radius, in the approximate location of the maximum gradient in time-averaged electron density. This is likely the cause of the marked broadening of the density profiles at the onset of the instability seen in previous studies.[11]

The results shown here correspond to a single condition, and so are not extensible to the entire range of device operation. Similar experiments were performed for a range of discharge conditions and will be described in forthcoming work.

A model of the instability is the focus of ongoing investigations. We may note substantial similarities between the observed oscillations with the modified Simon-Hoh instability of Sakawa,[13] as well as the spoke-type ionization instability found in $\mathbf{E} \times \mathbf{B}$ devices, such as Hall thrusters[19,27,28] and magnetrons.[23,29] The latter case presents interesting prospects for relating these instabilities to the anomalously high ion energies observed in hollow cathode discharges.[5,30] Ultimately, a device level model is desired that can capture the cross-field transport of electrons self-consistently, allowing us to have a truly well-defined plasma source for material interactions experiments, as well as for probe theory and code validation.

Acknowledgments

This work is funded by the U.S. Air Force Office of Scientific Research under grant no. FA9550-11-1-0282 and the UCLA School of Engineering and Applied Sciences.

References

[1]S. Yoshikawa and D. J. Rose. Anomalous Diffusion of a Plasma across a Magnetic Field. *Physics of Fluids*, 5(May 2015):334, 1962.

[2]D. L. Morse. Plasma rotation in a hollow cathode discharge. *The Physics of Fluids*, 8(3):516–521, 1965.

[3]J. H. Noon, H. A. Schmidt, and E. H. Holt. Connection between self-excited low frequency oscillations and anomalous plasma diffusion. *Plasma Physics*, 12:477–488, 1970.

[4]G. M. Wheeler and R. V. Pyle. Wave enhanced transport in an arc discharge. *Plasma Physics*, 16:909–919, 1974.

[5]D. M. Goebel, K. K. Jameson, I. Katz, and I. G. Mikellides. Potential fluctuations and energetic ion production in hollow cathode discharges. *Physics of Plasmas*, 14(103508):1–15, 2007.

[6]B. A. Jorns, I. G. Mikellides, and D. M. Goebel. Temporal Fluctuations in a 100-A LaB 6 Hollow Cathode. In *33rd International Electric Propulsion Conference*, 2013.

[7]B. A. Jorns and Richard R. Hofer. Plasma oscillations in a 6-kW magnetically shielded Hall thruster. *Physics of Plasmas*, 21, 2014.

[8]G. Guest and A. Simon. Instability in Low-Pressure Plasma Diffusion Experiments. *Physics of Fluids*, 5(May 2015):503, 1962.

[9]F.C. Hoh. Instability of Penning-type discharges. *The Physics of Fluids*, 6(8):1184–1191, 1963.

[10]T. S. Matlock, D. M. Goebel, R. Conversano, and R. E. Wirz. A dc plasma source for plasma material interaction experiments . *Plasma Sources Science and Technology*, 23(2), 2015.

[11]T. S. Matlock, D. M. Goebel, and R. E. Wirz. Near anode plasma in the plasma interaction facility at UCLA. In *33rd International Electric Propulsion Conference*, 2013.

[12]T. S. Matlock, D. M. Goebel, and R. E. Wirz. An Investigation of Low Frequency Plasma Instabilities in a Cylindrical Hollow Cathode Discharge. In *50th AIAA/ASME/SAE/ASEE Joint Propulsion Conference and Exhibit*, Cleveland, OH, 2014.

[13]Y. Sakawa, C. Joshi, P. K. Kaw, F. F. Chen, and V. K. Jainb. Excitation of the modified Simon-Hoh instability in an electron beam produced plasma. *Physics of Fluids B*, 5(6):1681, 1993.

[14]A. Fruchtman, D. Zoler, and G. Makrinich. Potential of an emissive cylindrical probe in plasma. *Physical Review E*, 84(2):025402, August 2011.

[15]J. P. Sheehan, Y. Raitses, N. Hershkowitz, I. Kaganovich, and N. J. Fisch. A comparison of emissive probe techniques for electric potential measurements in a complex plasma. *Physics of Plasmas*, 18(7):073501, 2011.

[16]T. S. Matlock. On the use of electrostatic probes for plasma instability measurements. 2015.

[17]A. H. Nielsen, H. L. Pecseli, and J. Juul Rasmussen. Turbulent transport in low-β plasmas. *Physics of Plasmas*, 3(1996):1530, 1996.

[18]A. W. Smith and M. A. Cappelli. Time and space-correlated plasma potential measurements in the near field of a coaxial Hall plasma discharge. *Physics of Plasmas*, 16, 2009.

[19]C. L. Ellison, Y. Raitses, and N. J. Fisch. Cross-field electron transport induced by a rotating spoke in a cylindrical Hall thruster. *Physics of Plasmas*, 19:1–7, 2012.

[20]K. Chung. Mach probes. *Plasma Sources Science and Technology*, 21:63001, 2012.

[21]R. C. Davidson. Vlasov equilibrium and nonlocal stability properties of an inhomogeneous plasma column. *Physics of Fluids*, 19(8):1189–1202, 1976.

[22]J. M. Beall. Estimation of wavenumber and frequency spectra using fixed probe pairs. *Journal of Applied Physics*, 53(6):3933, 1982.

[23]N. Brenning, D. Lundin, T. Minea, C. Costin, and C. Vitelaru. Spokes and charged particle transport in HiPIMS magnetrons. *Journal of Physics D: Applied Physics*, 46:084005, 2013.

[24]R. B. Lobbia and A. D. Gallimore. A Method of Measuring Transient Plume Properties. Number July, pages 1–15, 2008.

[25]R. W. Motley. Hot-probe measurements of space potential oscillations in a plasma. *Journal of Applied Physics*, 43(1972):3711, 1972.

[26]S. Klose, W. Bohmeyer, M. Laux, and H. Meyer. Investigation of Ion Drift Waves in the PSI-2 Using Langmuir -Probes. *Contributions to Plasma Physics*, 41(5):467–472, 2001.

[27]G. S. Janes and Lowder R. S. Anomalous Electron Diffusion and Ion Acceleration in a Low-Density Plasma. *The Physics of Fluids*, 9(6):1115–1123, 1966.

[28]D. Escobar and E. Ahedo. Global stability analysis of azimuthal oscillations in Hall Thrusters. *33rd International Electric Propulsion Conference*, pages IEPC–2013–304, 2013.

[29]A. Anders, P. Ni, and A. Rauch. Drifting localization of ionization runaway: Unraveling the nature of anomalous transport in high power impulse magnetron sputtering. *Journal of Applied Physics*, 111(May), 2012.

[30]I. Kameyama and P. J. Wilbur. Effects of external flow near high-current hollow cathodes on ion-energy distributions. In *International Electric Propulsion Conference*, pages 1053–1060, 1997.